Design and numerical aerodynamic analysis of a centrifugal compressor impeller for a 100 kgf-thrust gas turbine engine

Trinh Phan Anh[1], Khuat Cao Khai[2], Dinh Cong Truong[1*]

[1]School of Mechanical Engineering, Hanoi University of Science and Technology, 1 Dai Co Viet, Bach Mai, Hanoi, Vietnam.
[2]Institute of Missile, Academy of Military Science and Technology, 17 Hoang Sam, Nghia Do, Hanoi, Vietnam.
[*]Corresponding author: truong.dinhcong@hust.edu.vn
Received 10 Feb. 2026; Revised 6 Apr. 2026; Accepted 10 Apr. 2026; Published 25 Apr. 2026.
DOI: https://doi.org/10.54939/1859-1043.j.mst.110.2026.159-168

ABSTRACT

Small gas turbine engines with 100 kg thrust are increasingly used in unmanned aerial vehicles (UAVs) and small aerospace propulsion systems. In these engines, centrifugal compressors are preferred for their compact design, high compression ratio, and high isothermal efficiency. This study presents the preliminary design and computational fluid dynamics (CFD)-based aerodynamic investigation of a centrifugal compressor impeller. A complete three-dimensional geometry was developed from the target operating parameters, and Reynolds-averaged Navier-Stokes simulations with k-SST turbulence modeling were performed to analyze the internal flow field and evaluate the impeller's aerodynamic performance. The numerical results showed that the total pressure ratio and efficiency were 4.505 and 85.007% at the design point, and the near-stall margin achieved at 18.056% within the typical requirements of a gas turbine engine compressor.

Keywords: Small gas turbine engine; Centrifugal compressor; Impeller; CFD; Aerodynamic characteristics.

1. INTRODUCTION

Small gas turbine (SGT) engines have gained increasing attention in recent years due to their compact size, high rotational speed, and suitability for a wide range of aerospace applications such as UAVs, small rockets, and small aerospace propulsion systems. In these engines, the compressor plays a crucial role as the first component to interact with the incoming airflow and generate the pressure boost necessary for efficient combustion. Therefore, the compressor's performance strongly influences thrust generation, fuel efficiency, and operational stability.

For engines with thrust around 100 kgf, centrifugal compressors are widely used because they can achieve relatively high pressure ratios in a single stage while maintaining a compact and mechanically simple configuration. These characteristics make centrifugal compressors particularly suitable for small propulsion systems where space and weight constraints are critical [1, 2]. Among the components of a compressor, the impeller is the most influential factor in determining aerodynamic performance, as it regulates the energy transfer to the working fluid and controls the flow supplied to the diffuser [3-6]. Despite the increasing importance of SGT, detailed studies in the open literature on centrifugal compressor impeller design for this type of thrust remain limited [7]. The lack of publicly available design procedures is the driving force behind the current research.

Therefore, this paper focuses on the design and aerodynamic investigation of a centrifugal compressor's impeller for a 100 kgf-thrust SGT. The primary objective is to establish a basic design workflow, ranging from preliminary mean-line calculations to complete 3D geometry generation, followed by the implementation of a Reynolds-Averaged Navier-Stokes (RANS)-based CFD model to examine the internal flow field. The study analyzes characteristic loss mechanisms, including tip clearance leakage, adverse pressure gradients, and the radial distribution of velocity and pressure, while assessing the impeller's ability to achieve target

pressure ratios and efficiency at the design point. Simultaneously, this work paves the way for the impeller design phase in the development of SGTs.

2. DESIGN METHODOLOGY OF A CENTRIFUGAL COMPRESSOR IMPELLER FOR A 100 KGF-THRUST GAS TURBINE ENGINE

2.1. Main parameters of 100 kgf-thrust gas turbine engines

Technical data regarding gas turbine engines in the 100-kgf thrust class is relatively scarce due to defense and security restrictions. To obtain a comprehensive understanding of the geometric and operating parameters from reputable manufacturers, two types of turbine engines, PBS TJ100 (Czech Republic) and JetCat P1000 (Germany), were selected for investigation. Their primary operating parameters are summarized in Table 1 (under ISA conditions: Temperature of 15 °C, atmospheric pressure of 101.325 kPa, and wind speed of 0 m/s).

Table 1. *The main operating parameters of gas turbine engines in the 100 kgf thrust class.*

Main operating parameters / Turbine engines	Maximum rotational speed (rpm)	Outer diameter (mm)	Mass (kg)	Maximum thrust (N)	Mass flow rate at design point (kg/s)
PBS TJ100 (PBS, CH-Czech) [8]	60 600	272	17.6	1320	2,0
Jetcat P1000 [9]	61500	234	11	1100	1,8

Based on the survey of the main operating parameters of gas turbine engines in the 100 kgf thrust class, it is observed that the centrifugal compressors in this class of turbine engines operate at relatively high rotational speeds (ranging from 60600 rpm to 61500 rpm), with a design-point mass flow rate reaching approximately 2.0 kg/s (PBS TJ100), and with an outer diameter in the range of 234 mm to 272 mm (in relation to these types of engines' power generation capability). Additionally, the design-point pressure ratio of the centrifugal compressor in Jetcat P1000 is 4.0, as reported in the manufacturer's published brochure [9].

Although the efficiency values of centrifugal compressors used in 100 kgf-thrust turbine engines have not been published, based on other small gas turbine engines, the compressor efficiency typically ranges from 77% to 86.9% when measured under laboratory conditions or estimated using predictive models [10-13].

Based on the aforementioned reference parameters, and in order to ensure stable compressor operation, the impeller's principal operating parameters were selected with design values slightly higher than the reference ranges (excluding the reduction in rotational speed to suit the increased compressor power). Therefore, the main operating parameters adopted for the design of the centrifugal compressor's impeller for the 100 kgf-thrust gas turbine engine are as follows: Rotational speed = 57300rpm; Mass flow rate target (M target) = 2.2 kg/s; Pressure ratio target (PR target) = 4.5; Total-to-total isentropic efficiency target (EFF target) = 85%.

2.2. Design

The number of impeller blades is calculated following the empirical correlation proposed by Wiesner (1967) [14]:

$$\sigma = 1 - \frac{\sqrt{\cos\beta_2}}{Z^{0.7}} \quad (1)$$

Where: σ: Slip factor; β_2: Blade angle to the meridional direction at the impeller outlet, Z: Number of impeller blades. Based on the prediction model of Busemann and experimental results,

the slip factor is selected $\sigma = 0.9$ to min0imize the slip of the airflow relative to the impeller blades. β_2 is assumed: 55˚ (was preliminarily selected within the recommended range reported in Reference [14]). Z is calculated as approximately 18.25. The impeller typically consists of main blades and splitter blades arranged alternately to mitigate inlet flow blockage while maintaining adequate flow guidance at the outlet [15]. Accordingly, the total number of blades (Z) is selected as 18, comprising 9 main blades and 9 splitter blades.

"René Van den Braembussche" proposed several design ratios to ensure the stable operation of the impeller, as summarized in Table 2.

Table 2. *Recommended ranges of design ratios.*

Design ratios	R_{1S}/R_2	b_2/R_2	R_{1H}/R_{1S}	β_{1S}	β_2	$(l_m - l_s)/ l_m$	c/b_2
Recommended ranges	0.5-0.8	0.05-0.15	0.3-0.7	50˚-60˚	40˚- 60˚	0.2-0.35	0.026-0.155

Where: R_{1H}: Leading-edge radius at the hub; R_{1S}: Leading-edge radius at the shroud; R_2: Outer radius at the trailing edge; b_2: Impeller outlet with; β_{1S}: Blade angle at the impeller inlet at the shroud relative to the meridional direction; l_m: Length of main blade; l_s: Length of splitter blade; c: Tip clearance) [14, 16].

Based on the design operating parameters, Cfturbo commercial software [17] generates preliminary geometric parameters for the impeller. However, empirical formulas and integrated prediction models within the software often struggle to produce a comprehensive 3D model that completely satisfies 1D design targets and other critical operational criteria, such as a proper Surge Margin (SM). Therefore, Computational Fluid Dynamics (CFD) is utilized as the initial basis for verification and subsequent calibration. After several design iterations (guided by the influence of geometric parameters on impeller characteristics [14]), a set of main geometry parameters satisfying the design criteria and the aforementioned ratios is summarized in Table 3 and illustrated in Figure 1.

Table 3. *Main geometry parameters of the impeller.*

Z	R_{1H} (mm)	R_{1S} (mm)	R_2 (mm)	b_2 (mm)	β_{1S}	β_2	l_m (mm)	l_s (mm)	c (mm)
18	19.5	61.8	94.5	11.2	59˚	55˚	65	43	0.5

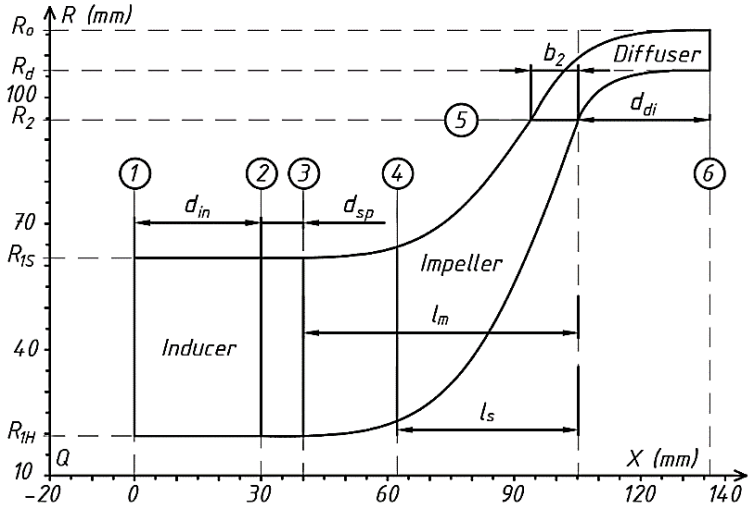

Figure 1. *Meridional cross-section of the compressor.*

The QXR coordinate system is defined with the QX-axis aligned axially. The positive direction follows the inflow toward the compressor, where the first plane of contact with the incoming flow (plane (1)) is set at a coordinate of 0 mm.

The QR-axis is oriented in the radial direction, with its values representing the distance from the compressor's centerline.

Where: d_{in}: Length of inducer; d_{sp}: Distance from the flow field region tends to move axially to the main blade leading edge; d_{di}: Length of the diffuser hub; R_d: Radius of outer hub diffuser; R_o: Radius of outer shroud diffuser.

The inducer domain starts from plane (1) to plane (2); the impeller domain starts from plane (2) to plane (5); the diffuser domain starts from plane (5) to plane (6). (The geometric parameters of the inducer and diffuser domains were selected to relatively correlate with the impeller).

3. NUMERICAL ANALYSIS

3.1. Grid generation and simulation setup

During mesh generation in ANSYS TurboGrid® 2025 R1 [18], based on the three-dimensional geometry exported from Cfturbo [17], structured hexahedral elements are employed for the centrifugal compressor domain. Meshing is performed to ensure an appropriate y+ value, which is critical for the accuracy of the model's numerical results. The rotating domain of the impeller was extended to a radius 2.5 mm larger than the impeller tip radius R_2 [19].

A mesh independence study was performed to balance accuracy and computational efficiency by analyzing the sensitivity of the pressure ratio to mesh density.

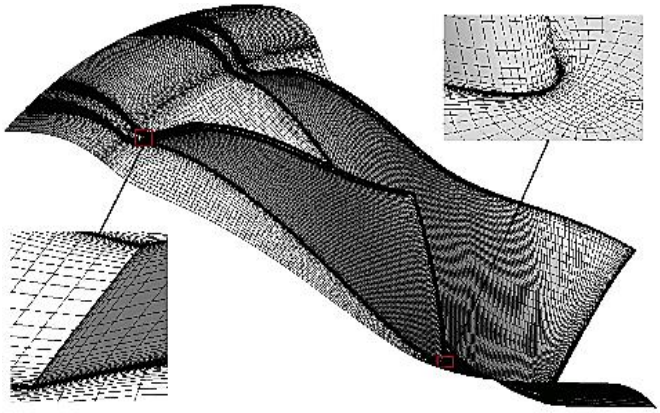

Figure 2. *Aerodynamic mesh of the impeller blades.*

Figure 2 illustrates the impeller mesh results, highlighting the refined grid density in critical regions such as the hub and shroud regions (where tip leakage occurs, a phenomenon significantly impacting compressor efficiency). With a tip clearance set at 0.5 mm, the mesh in this area is locally refined to accurately capture the characteristics of the leakage flow.

The grid structure along the blade tips yields stable numerical solutions, especially for high-speed simulations (57300 rpm) where flow fields are highly turbulent and prone to significant flow separation. The y+ value is under 5 to ensure effective boundary layer modeling.

The k–ω SST (k-omega Shear Stress Transport) turbulence model is adopted for the present simulations. This model provides accuracy in predicting adverse pressure-gradient flows and near-wall behavior, which are essential in centrifugal compressor impellers. Under stable operating conditions, a steady-state approach is considered adequate for preliminary geometric assessment and for investigating performance characteristics (pressure ratio and efficiency) and aerodynamic phenomena.

Convergence is assumed when the root mean square (RMS) residuals of the continuity, momentum, and turbulence transport equations decrease below 10^{-6}, while the inlet and outlet mass flow rates are simultaneously monitored to ensure global conservation [20].

3.2. Characteristic equations for the impeller

To evaluate the aerodynamic effectiveness and thermodynamic performance of the impeller, formulas are used as follows [20]:

Total Pressure Ratio (PR) and Temperature Ratio (TR):

$$PR = \frac{P_{t2}}{P_{t1}} \; ; \; TR = \frac{T_{t2}}{T_{t1}} \tag{2}$$

Where: P_{t2}, P_{t1}: Total pressure at the outlet and inlet of the impeller, respectively. T_{t2}, T_{t1}: Mass-flow-averaged total temperature at the outlet and inlet of the impeller, respectively.

Total-to-total isentropic efficiency (EFF):

$$EFF = \frac{PR^{\frac{k-1}{k}} - 1}{TR - 1} \; ; \; k = \frac{C_p}{C_v} \tag{3}$$

Where: k is the specific heat ratio of the working fluid; C_p, C_v: Specific heats at constant pressure and constant volume, respectively. In the boundary conditions: $C_p \approx 1005$ J/Kg.K; $C_v \approx 718$ J/Kg.K; Substituting the values $k \approx 1.4$.

To evaluate the stable operating range of the impeller, the surge margin (SM) is calculated as:

$$SM = \left[\frac{PR_{sur} / m_{sur}}{PR_{ds} / m_{ds}} - 1 \right] \times 100\% \tag{4}$$

Where: P_{sur}, m_{sur} : Impeller pressure ratio and mass flow rate at surge stage, respectively; P_{ds}, m_{ds}: Impeller pressure ratio and mass flow rate at design point, respectively.

3.3. Boundary conditions

The primary types of boundary conditions include: Wall boundaries, inlet, and outlet boundaries. The main boundary conditions for the model are presented in Table 4.

Table 4. *Boundary conditions.*

Analysis type	Steady State	
Domain motion	Inducer, Diffuser	Stationary
	Impeller	Rotating
Inlet conditions	Inlet total pressure	1 atm
	Inlet total temperature	288.15 K
	Inlet turbulence intensity	5%
Outlet conditions [21]	Average static pressure	Variable
	Mass flow rate	
Rotational speed	57300 rpm	
Fluid type	Ideal gas	
Interface model	Rotational Periodic	
Frame change/Mixing model	Mixing Plane	
Wall conditions	No-slip, adiabatic, and smooth wall	
Turbulence model	k–ω SST	
Reynolds number	2.10^6	

4. RESULT AND DISCUSSION

4.1. Mesh independence

To ensure that the simulation results are independent of the mesh refinement level, five different mesh scales were surveyed, as shown in Figure 3.

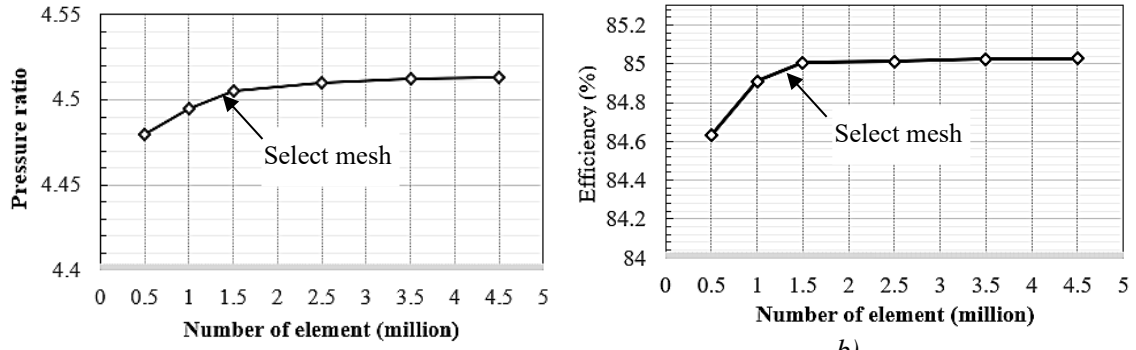

a) *b)*

Figure 3. *Mesh independence at the design point.*

In these plots, the horizontal axis represents the number of mesh elements (in millions), while the vertical axis represents the mass flow rate (Figure 3a) and efficiency (Figure 3b). With an error of 0.17% in pressure ratio and 0.03% in efficiency when the mesh size was increased from 1.5 to 4.5 million elements, while the error increased significantly (0.55% in pressure ratio and 0.4% in efficiency) when the mesh was reduced to 0.5 million elements, a mesh comprising 1.5 million elements was therefore selected to balance numerical accuracy and computational cost.

4.2. Comparison between proposed characteristics and main operating parameter targets

The main operating characteristics investigated on the impeller from plane (2) to plane (3) (as shown in Figure 1) are presented in Figure 4.

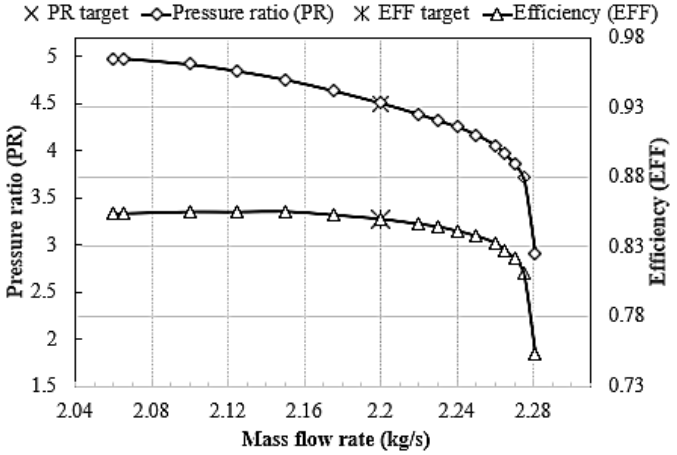

Figure 4. *Main operating characteristics of the impeller.*

At the design point (the mass flow rate = M target), the pressure ratio (PR) and efficiency (EFF) reach 4.505 (0.11% error) and 85.007% (0.008% error), respectively. At the near-stall point, the mass flow rate is 2.06 kg/s with a pressure ratio of 4.98. Substituting these values into equation (4), the Surge Margin (SM) is approximately 18.056%, which falls within the typical range of 10% to 20% for gas turbine engines [22]. Although the design efficiency of 85.007% at 2.2 kg/s is slightly lower than the peak efficiency of 85.552% (at the mass flow rate of 2.15 kg/s), the difference is approximately 0.6%. Thus, the impeller's performance remains adequately effective and satisfies the design requirements.

4.3. Aerodynamic characteristics analysis

Figures 5, 6, 7, 8, illustrate the total pressure and relative Mach number contours on the blade-to-blade and meridional planes for three operating conditions: (a) choke, (b) design point, and (c) near stall.

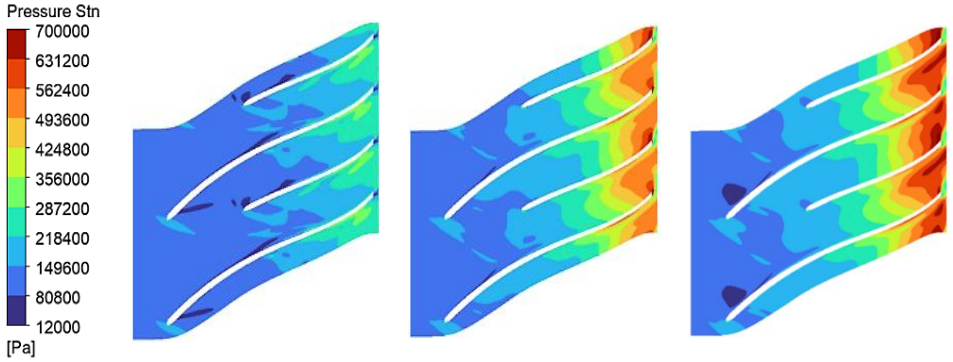

a) *b)* *c)*

Figure 5. *Total pressure distribution on the blade-to-blade view (at mid span).*

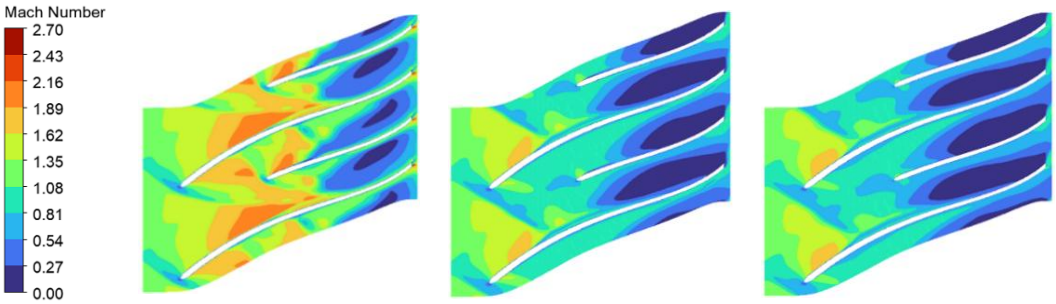

a) *b)* *c)*

Figure 6. *Relative Mach number distribution on the blade-to-blade view (at mid span).*

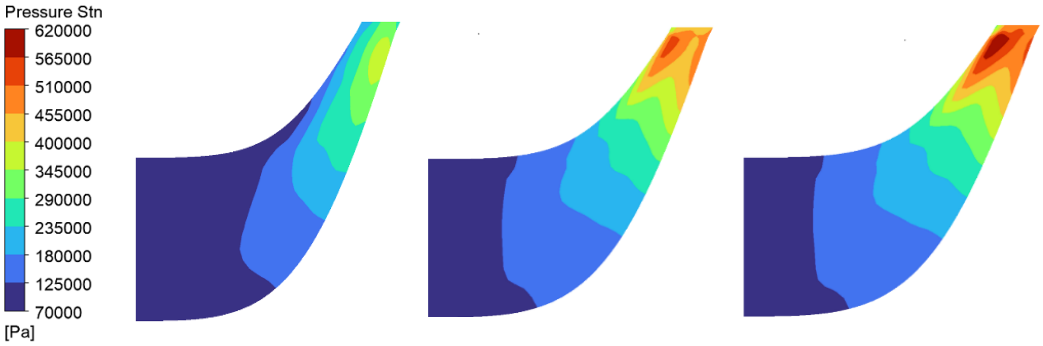

a) *b)* *c)*

Figure 7. *Total pressure distribution on the meridional view.*

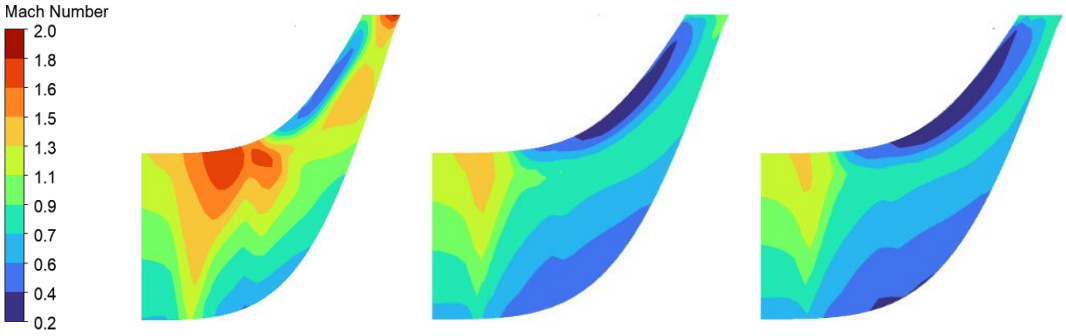

a) *b)* *c)*

Figure 8. *Relative Mach number distribution on the meridional view.*

In general, it is observed that as the operating condition shifts from choke to near stall conditions, the total pressure distribution exhibits a progressive increase, while the relative Mach number distribution shows a downward trend. At the near-stall condition (Figures 5c, 7c), local high-pressure peaks of approximately 6.10^5 Pa are observed at the trailing edge. This causes a non-uniform pressure distribution at the outlet, increasing the potential for backflow or recirculation vortices. At the choke condition (Figures 6a, 8a), a high-velocity region with a Mach number of nearly 2.0 extends across from the main-blade leading edge to the splitter-blade leading edge. This broad supersonic zone indicates the occurrence of flow choking at the impeller inlet. In figures 6 and 8, the low velocity region at the impeller shroud expands as the operating condition shifts from choke to near stall conditions. At the near-stall point (Figure 6c), a low-velocity region (below Mach 0.27) tends to expand and lengthen along the trailing edge profile. This signifies the onset of near-stall phenomena, such as flow separation or blockage.

The streamlines of the impeller at three operating conditions ((a) choke, (b,d,e) design point, and (c) near stall) are illustrated in Figure 9. Overall, tip leakage flows are present in all three operating conditions. This phenomenon correlates with the low-Mach regions (below 0.4) observed at the trailing edge region, near the suction side (Figure 6c), and the trailing edge region, near the shroud surface (Figure 8c).

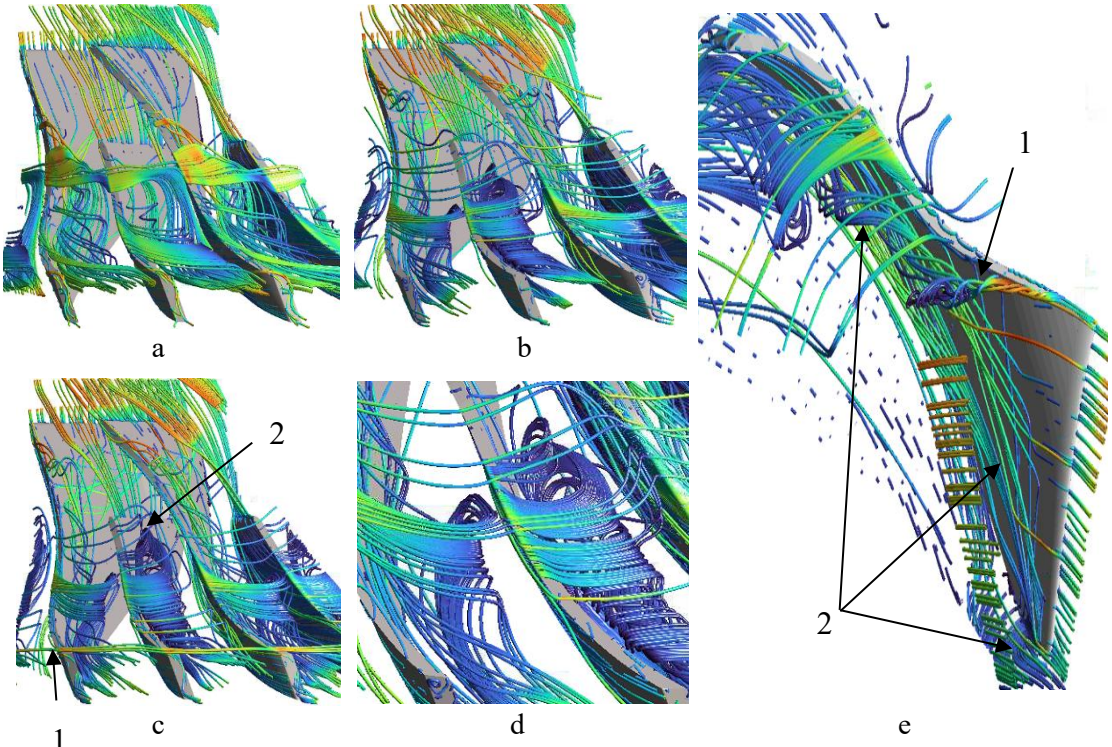

Figure 9. *Streamlines of the impeller.*

At the near-stall condition (Figure 9c), flow separation and vortices become more pronounced with increased turbulence intensity. Notably, a circumferential vortex pattern (labeled '1' in Figure 9c) is observed (a distinctive characteristic of the stall condition [23]).

Additionally, other flow patterns commonly developed within centrifugal compressor impellers are observed at the design point include the wake secondary flow (Figure 9d), as well as the tip corner vortex (labeled '1' in Figure 9e) and the hub corner vortex (labeled '2' in Figure 9e) [24].

Moreover, under near-stall conditions, the more intensified development of the wake secondary flow toward the splitter-blade leading edge (labeled '2' in Figure 9c) (compared to the design point

in Figure 9b) results in a local low-relative-Mach region (below 0.4) at the hub of the splitter leading edge (Figure 8c).

5. CONCLUSIONS

This paper presents the design process and numerical simulation of the aerodynamic characteristics of a centrifugal compressor impeller for a 100 kgf-thrust small gas turbine engine. From the design parameters (2.2 kg/s; PR = 4.5; EFF = 85% at 57,300 rpm), a 3D geometric model of the impeller was developed and evaluated using RANS simulations with k–ω SST turbulence model. At the design point, the impeller achieved a compression ratio of 4.505 and an efficiency of 85.007%, with very little deviation from the target values; the near stall point appeared at 2.06 kg/s with PR 4.98, corresponding to a surge margin of approximately 18.056%, within the typical requirements of a gas turbine engine compressor. Flow field analysis at choke, design point, and near-stall conditions reveals aerodynamic mechanisms dominating performance degradation, including inlet choking characterized by an extended high-Mach region (nearly Mach 2), persistent tip-leakage-related low-Mach zones near the shroud and trailing edge, and increasingly pronounced separation and vortex structures toward stall (wake secondary flow and corner vortices). Overall, the proposed design workflow and validated aerodynamic characteristics provide a practical basis for subsequent refinement and stage-level development of 100 kgf-class small gas turbine centrifugal compressors. Furthermore, this study paves the way for the comprehensive development of a 100 kgf-class gas turbine engine, as well as for further investigations into the design of other centrifugal compressors employed in small gas turbine engines.

REFERENCES

[1]. H. Krain, *"Review of centrifugal compressor's application and development"*, Journal of Turbomachinery, 127, 1, 25–34, (2005).

[2]. S. M. Hosseini, G. Najafi, B. Ghobadian, R. Mamat, *"Effects of radial gap ratio between impeller and vaned diffuser on performance of centrifugal compressors"*, Applied Sciences, 7, 7, 728, (2017).

[3]. C. Xu, R. S. Amano, *"Empirical design considerations for industrial centrifugal compressors"*, International Journal of Rotating Machinery, 2012, 184061, (2012).

[4]. S.-Y. Cho, K.-Y. Ahn, Y.-D. Lee, Y.-C. Kim, *"Optimal design of a centrifugal compressor impeller using evolutionary algorithms"*, Mathematical Problems in Engineering, 2012, 752931, (2012).

[5]. M. Casey, C. Robinson, *"Radial flow turbo compressors: Design, analysis, and applications"*, Cambridge University Press, (2021).

[6]. L. H. Jawad, S. Abdullah, R. Zulkifli, W. M. F. W. Mahmood, *"Numerical study on the effect of interaction vaned diffuser with impeller on the performance of a modified centrifugal compressor"*, Journal of Mechanics, 30, 2, 113–121, (2014).

[7]. M. Arifin *et al.*, *"Surrogate-based optimization of multiple-splitters radial compressor for solar hybrid microturbine"*, Energy Conversion and Management, 16, 100332, (2022).

[8]. PBS Group, *"PBS TJ 100-PBS Turbine Engine Portfolio"*, Czech Republic, (2021).

[9]. JetCat GmbH, *"JetCat pro engines"*, Germany, (2024).

[10]. Joaquín Valencia Bravo, Frederick Just Agosto, David Serrano Acevedo, Marco Menegozzo, *"Analytical modeling of characteristic maps of the SR-30 turbojet engine"*, International Journal of Engineering Research & Technology, 10, 3, 155–166, (2021).

[11]. Hamed MohamedAhmed Ali, Abdallah Almadani Muhammad Alhassan, Abdelrazig Abdelfadail Abdelrazig, Alla aldeen Ismail Massar, Muhammed Musa Haroun, *"Centrifugal compressor and bell mouth air intake preliminary design for micro turbojet engine"*, Journal of Karary University for Engineering and Science, 1, 2, (2021).

[12]. H. Krain, B. Hoffmann, H. Pak, *"Aerodynamics of a centrifugal compressor impeller with transonic inlet conditions"*, Proceedings of ASME Turbo Expo 1995: Power for Land, Sea, and Air, Houston, 95-GT-079, (1995).

[13]. Emilie Sauret, *"Open design of high pressure ratio radial-inflow turbine for academic validation"*, ASME International Mechanical Engineering Congress and Exposition, 7, 3183–3197, (2012).

[14]. René Van den Braembussche, *"Design and analysis of centrifugal compressors"*, von Karman Institute, ASME Press and John Wiley & Sons Ltd, (2018).
[15]. S. Pakle, K. Jiang, *"Design of a high-performance centrifugal compressor with new surge margin improvement technique for high-speed turbomachinery"*, Propulsion and Power Research, 7, 1, 19–29, (2018).
[16]. Jaatinen-Värri, J. Tiainen, T. Turunen-Saaresti, A. Grönman, A. Ameli, A. Engeda, J. Backman, *"Centrifugal compressor tip clearance and impeller flow"*, Journal of Mechanical Science and Technology, 30, 11, 5029–5040, (2016).
[17]. CFTurbo GmbH, *"CFTurbo user manual"*, Germany, (2024).
[18]. Ansys, *"Ansys TurboGrid user's guide"*, Canonsburg, PA, USA, (2025).
[19]. Y. P. Shum, C. S. Tan, N. A. Cumpsty, *"Impeller-diffuser interaction in a centrifugal compressor"*, ASME Journal of Turbomachinery, 122, 4, 777–786, (2000).
[20]. C. T. Dinh, *"Aerodynamic performance optimization of a transonic single-stage axial compressor using air bleeding, feedback, and injection"*, Ph.D. dissertation, Inha University, South Korea, 16, (2017).
[21]. A. Gibson, N. Gourdain, X. Ottavy, *"Assessment of turbulence model predictions for a centrifugal compressor simulation"*, Journal of the Global Power and Propulsion Society, 1, 1, 142–156, (2017).
[22]. H. I. H. Saravanamuttoo *et al.*, *"Gas turbine theory"*, Pearson Prentice Hall, (2009).
[23]. Q. Zhang, L. Zhang, Q. Huo, L. Zhang, *"Study on two types of stall patterns in a centrifugal compressor with a wide vaneless diffuser"*, Processes, 8, 10, 1251, (2020).
[24]. H. M. Harrison III, *"Development and validation of a new method to model slip and work input for centrifugal compressors"*, Ph.D. dissertation, Purdue University, (2020).

TÓM TẮT

Thiết kế và nghiên cứu đặc tính khí động bằng mô phỏng số của bánh công tác máy nén ly tâm cho động cơ tua-bin khí lực đẩy 100 kgf

Các động cơ tuabin khí nhỏ với lực đẩy 100 kg ngày càng được sử dụng rộng rãi trong UAV và các hệ thống đẩy hàng không vũ trụ cỡ nhỏ. Trong các động cơ này, máy nén ly tâm được ưa chuộng do thiết kế nhỏ gọn, tỷ số nén cao và hiệu suất đẳng nhiệt cao. Nghiên cứu này trình bày thiết kế sơ bộ và điều tra khí động học dựa trên CFD của cánh quạt máy nén ly tâm. Một hình học ba chiều hoàn chỉnh đã được phát triển từ các thông số hoạt động mục tiêu, và các mô phỏng Navier-Stokes trung bình theo Reynolds với mô hình nhiễu loạn k-SST đã được thực hiện để phân tích trường dòng chảy bên trong và đánh giá hiệu suất khí động học của bánh công tác. Kết quả tính toán số cho thấy tại điểm thiết kế, tỷ số áp suất toàn phần và hiệu suất lần lượt đạt 4,505 và 85,007%. Biên độ cận thất tốc đạt 18,056%, nằm trong phạm vi yêu cầu điển hình đối với máy nén của động cơ tuabin khí.

Từ khóa: Động cơ tuabin khí nhỏ; Máy nén ly tâm; Bánh công tác; CFD; Đặc tính khí động học.